Geoscience Frontiers 11 (2020) 439–450

Contents lists available at ScienceDirect

Geoscience Frontiers

journal homepage: www.elsevier.com/locate/gsf

Research Paper

Effect of mineralogy on friction-dilation relationships for simulated faults: Implications for permeability evolution in caprock faults

Fengshou Zhang [a,b], Mengke An [a,b], Lianyang Zhang [c,*], Yi Fang [d], Derek Elsworth [e,f]

[a] Key Laboratory of Geotechnical & Underground Engineering of Ministry of Education, Tongji University, Shanghai 200092, China
[b] Department of Geotechnical Engineering, Tongji University, Shanghai 200092, China
[c] Department of Civil and Architectural Engineering and Mechanics, University of Arizona, Tucson, AZ, 85721, USA
[d] Institute for Geophysics, Jackson School of Geosciences, The University of Texas at Austin, Austin, TX, 78712, USA
[e] Department of Energy and Mineral Engineering, EMS Energy Institute and G3 Center, The Pennsylvania State University, University Park, PA, 16802, USA
[f] Department of Geosciences, The Pennsylvania State University, University Park, PA, 16802, USA

ARTICLE INFO

Handling Editor: Christopher J Spencer

Keywords:
Fault gouge
Mineralogy
Strength and stability
Frictional healing
Gouge dilation
Permeability

ABSTRACT

This paper experimentally explores the frictional sliding behavior of two simulated gouges: one, a series of quartz–smectite mixtures, and the other, powdered natural rocks, aiming to evaluate and codify the effect of mineralogy on gouge dilation and frictional strength, stability, and healing. Specifically, velocity-stepping and slide-hold-slide experiments were performed in a double direct shear configuration to analyze frictional constitutive parameters at room temperature, under normal stresses of 10, 20, and 40 MPa. Gouge dilation was measured based on the applied step-wise changes in shear velocity. The frictional response of the quartz–smectite mixtures and powdered natural rocks are affected by their phyllosilicate content. Frictional strength and healing rates decrease with increasing phyllosilicate content, and at 20 wt.% a transition from velocity-weakening to velocity-strengthening behavior was noted. For both suites of gouges, dilation is positively correlated with frictional strength and healing rates, and negatively correlated with frictional stability. Changes in the permeability of gouge-filled faults were estimated from changes in mean porosity, indexed through measured magnitudes of gouge dilation. This combined analysis implies that the reactivation of caprock faults filled with phyllosilicate-rich gouges may have a strong influence on permeability evolution in caprock faults.

1. Introduction

Massive fluid injection for the stimulation of shale and enhanced geothermal reservoirs, and for the disposal and sequestration of wastewater and CO_2 may result in significantly elevated fluid pressures and the dynamic reactivation of pre-existing faults (Shapiro et al., 2006; Suckale, 2009; Elsworth et al., 2016; Grigoli et al., 2018; Kim et al., 2018; Yang et al., 2019). This reactivation is controlled by the frictional behavior of faults, and may be seismic or aseismic (Rutqvist et al., 2007; Guglielmi et al., 2015). Research in this area has attempted to create high permeability reservoirs while preserving the integrity of upper caprocks (Faoro et al., 2009; Zhong et al., 2016; Fang et al., 2017b; Im et al., 2018). Therefore, it is vital to examine the various friction–permeability relationships that have important implications for both, the sealing of caprocks and the recovery of unconventional resources.

Previous experiments showed that mineral composition affects the frictional properties of faults (Collettini et al., 2009; Faulkner et al., 2010; Ikari et al., 2011). For example, the frictional strength of faults were approximated with phyllosilicate content (Niemeijer and Spiers, 2006; Takahashi et al., 2007; Scuderi et al., 2013; Zhang et al., 2019). Low and high velocity experiments on fault gouges showed that phyllosilicate-rich faults exhibited a velocity-strengthening response that promoted stable frictional sliding (Saffer and Marone, 2003; Han et al., 2007; Kohli and Zoback, 2013; Boulton et al., 2017). Frictional healing is also significantly controlled by mineralogy (Chen et al., 2015; Carpenter et al., 2016); this can be partially explained by the crystalline structure of minerals, as well as fault loading conditions like humidity, temperature, chemical composition, and applied stresses (Kawamoto and Shimamoto, 1998; Frye and Marone, 2002; Tembe et al., 2010; Hunfeld et al., 2017).

Experiments on powdered gouges have indicated that gouge dilation

* Corresponding author.
E-mail address: lyzhang@email.arizona.edu (L. Zhang).
Peer-review under responsibility of China University of Geosciences (Beijing).

https://doi.org/10.1016/j.gsf.2019.05.014
Received 29 June 2018; Received in revised form 1 February 2019; Accepted 23 May 2019
Available online 27 July 2019

is also strongly dependent on mineralogy (Marone and Kilgore, 1993; Ikari et al., 2009; Samuelson et al., 2009). Other representative studies for the relationship between dilation and mineralogy include Kohli and Zoback (2013) on powdered shale reservoir rocks, and Scuderi et al. (2013) on dolomite and anhydrite gouge. However, little attention has been paid to the correlation between gouge dilation and frictional properties, especially for healing response (Scuderi et al., 2014).

Permeability typically evolves during fracture shear as a result of dilation and compaction (Samuelson et al., 2009, 2011; Fang et al., 2017a; Ye et al., 2017). This observation may be used in estimating the change in permeability during fault shear by directly indexing permeability evolution to gouge dilation or compaction. Previous research only investigated the impact of mineralogy on the friction–permeability relationship of gouges under low normal stresses (generally <10 MPa) (Fang et al., 2018b), and it is necessary to evaluate this relationship at higher stresses (>10 MPa).

This paper (1) reports laboratory measurements of the influence of phyllosilicate content on frictional strength, stability and healing of simulated fault gouges; (2) assesses the relationships between fault gouge dilation and frictional strength, stability, and healing; and (3) applies these observations of friction–dilation to infer the permeability evolution of gouge present in caprock faults by directly indexing permeability with gouge dilation. The experiments conducted for this study used quartz–smectite mixtures and powdered natural rocks as simulated fault gouges.

2. Experimental methods

Velocity-stepping and slide-hold-slide experiments were conducted in a double-direct shear configuration on quartz–smectite mixtures and powdered (natural) reservoir rocks. Strength evolution data were used to project magnitudes of frictional strength, stability, and healing, and to infer the evolution of permeability.

2.1. Sample material

Synthetic quartz–smectite mixtures and powdered natural rocks were adopted as simulated fault gouges for friction tests. The quartz powders used were commercially available quartz sand with >98% purity; grain-sizes <150 μm were separated by sieving. The smectite powders were derived from sodium bentonite; grains <45 μm in size were separated by sieving through a 325-mesh. The fabricated quartz–smectite gouges span the entire 0–100 wt.% range. Natural rocks like the Daqing volcanic rocks (Songliao Basin), Shengli sandstone (Shandong Hills), Junggar clasolite and sandstone (Junggar Basin), Fuling shale, Changning shale and chlorite schist (Sichuan Basin) were used for these experiments. X-ray diffraction (XRD) results showed between 4 and 37 wt.% phyllosilicate content for these natural rock samples (Table 1). They were crushed and ground in a grinding machine to <150 μm grain-size.

2.2. Experimental procedure

All friction experiments were performed in a double direct shear configuration using a biaxial loading frame (Fig. 1), as per Johnson et al. (2008). Two identical 5-mm-thick gouge layers were sandwiched between three grooved stainless-steel platens, with a constant nominal area of 5 cm × 5 cm maintained throughout the experiment (Fig. 1b). A normal force is applied by a horizontal piston to the gouge layers, and a shear force is applied by moving the central steel platen with a vertical piston. The shear displacement and gouge layer thickness were measured by displacement sensors to a precision of ±0.1 μm, with the applied force recorded to ±0.5 kN via internal load cells.

Velocity-stepping and slide-hold-slide tests were carried out to measure frictional stability and healing, respectively, at three different normal stresses (Fig. 2, Table 2). All tests were performed at room temperature (25 °C). The tests on the quartz–smectite mixtures were carried out at natural room humidity (55%–65% relative humidity), while those on the powdered natural rocks were performed under water-saturated conditions. Water saturation was ensured throughout the experiment by placing the samples in a ziplock bag filled with deionized water for a minimum of 4 h. The tests were conducted while the sample was still in the ziplock bag, and the bag was arranged such that it did not affect the experiments, following the protocol established in Frye and Marone (2002), Samuelson et al. (2008), and Scuderi et al. (2014).

At the initiation of each velocity-stepping experiment, normal stress was established at 10 MPa, after which shear velocity was applied at 10 μm/s until a steady frictional state was achieved. The velocity was then stepped from 0.3 through 300 μm/s for the quartz–smectite mixtures, and 0.1 through 100 μm/s for the powdered natural rocks at each normal stress level (Fig. 2a). The velocity-stepping schedule was identical for all the prescribed normal stresses.

Different from the velocity-stepping tests, for the slide-hold-slide experiments, the shear velocity was set at 10 μm/s throughout the entire test duration; the hold time (the time for keeping the driving vertical piston steady) varied from 3 to 300 s for the quartz–smectite mixtures, and 1–1000 s for the powdered natural rocks. Holds were applied with every 0.5-mm-shear displacement (Fig. 2b). The final shear displacements were 20.5 mm for the quartz–smectite mixtures, and 16.5 mm for the powdered natural rocks, respectively.

2.3. Frictional parameters and gouge dilation

Frictional strength was evaluated from the coefficient of friction μ as:

$$\mu = \tau/\sigma_n \tag{1}$$

where τ is the measured shear stress and σ_n is the normal stress.

The velocity dependence of fault slip was analyzed on the basis of the rate and state friction as (Dieterich, 1978, 1979; Ruina, 1983; Marone, 1998):

$$\mu = \mu_0 + a\ln\left(\frac{V}{V_0}\right) + b_1\ln\left(\frac{V_0\theta_1}{D_{c1}}\right) + b_2\ln\left(\frac{V_0\theta_2}{D_{c2}}\right) \tag{2}$$

$$\frac{d\theta_i}{dt} = 1 - \frac{V\theta_i}{D_{ci}},\ i = 1,\ 2 \tag{3}$$

where μ_0 is the reference coefficient of friction at the reference shear velocity V_0; a, b_1, and b_2 are dimensionless friction parameters; θ_1 and θ_2 are state variables; D_{c1} and D_{c2} are critical slip distances, that reflect the slip distance for a new steady-state.

For a single velocity step (Fig. 3a), the frictional stability parameter $a - b$ was determined from Eqs. (2) and (3) ($\theta_i = D_{ci}/V$ at steady friction state) as (Marone, 1997):

$$a - b = \Delta\mu_{ss}/\ln(V/V_0) \tag{4}$$

where $b = b_1 + b_2$, and $\Delta\mu_{ss}$ is the change in steady-state friction coefficient during a step of shear velocity from V_0 to V. Positive values of $a - b$ denote velocity-strengthening and stable slip, while negative values of $a -$

Table 1
X-ray diffraction (XRD) mineral proportions (in wt.%) of gouges derived from the crushed natural rocks. Abbreviations: Qtz, quartz; Fsp, feldspar; Cal, calcite; Dol, dolomite; Ill, illite; Chl, chlorite. Phyllosilicates are predominantly illite and chlorite.

Rock samples	Qtz	Fsp	Cal	Dol	Ill	Chl	Phyllosilicates
Daqing volcanic rock	53	43	–	–	–	4	4
Shengli sandstone	33	18	8	33	7	1	8
Junggar clasolite	53	29	6	–	7	5	12
Junggar sandstone	47	36	–	–	12	5	17
Fuling shale	41	10	24	6	17	2	19
Changning shale	47	16	9	4	19	5	24
Chlorite schist	30	22	11	–	8	29	37

b indicate potentially unstable sliding behavior. All friction constitutive parameters were derived by inverse modeling by an iterative least squares method.

As established in previous studies (Ikari et al., 2009; Samuelson et al., 2009; Scuderi et al., 2013), gouge dilation Δh in velocity-stepping experiments, was defined as the change in gouge layer thickness resulting from a velocity step (Fig. 3b).

In slide-hold-slide tests (Fig. 3c), the frictional healing $\Delta\mu$ represented the difference between the previous steady-state coefficient of friction, and the peak coefficient of friction after reloading. The frictional healing rate β was the ratio of frictional healing $\Delta\mu$ and the logarithm of hold time t_h (Fig. 3d), expressed as:

$$\beta = \Delta\mu/\log_{10} t_h \quad (5)$$

3. Results

Experimental results showed that the frictional properties and dilation of both, the quartz–smectite mixtures and powdered natural rocks, were strongly dependent on their phyllosilicate content. Relationships between gouge dilation and fault strength, stability, and healing were established and are discussed in detail below.

3.1. Frictional strength and stability

Previous laboratory studies suggested that the frictional strength of simulated fault gouges is negatively correlated with their phyllosilicate content (Logan and Rauenzahn, 1987; Takahashi et al., 2007; Crawford et al., 2008; Tembe et al., 2010; Moore and Lockner, 2011); data from this study, for the quartz–smectite mixtures and powdered natural rocks at a normal stress of 20 MPa, agree with these assessments (Fig. 4). For the quartz–smectite mixtures, the steady-state coefficient of friction at shearing velocities of 0.3–300 μm/s is plotted in Fig. 4a. The coefficient of friction ranges from 0.4 to 0.8; here, the maximum and minimum values are for pure quartz and pure smectite, respectively. It exhibits a nearly linear trend with increasing phyllosilicate content, congruent with the observations by Tembe et al. (2010) on binary mixtures of quartz and smectite. The coefficient of friction of 0.4–0.43 for pure smectite gouge from this study is higher than those (0.1–0.3) from previous studies (Takahashi et al., 2007; Tembe et al., 2010), mainly due to the different humidity conditions maintained during the tests. In this study, experiments on the quartz–smectite mixtures were conducted at natural room humidity conditions, while those in the previous studies were carried out under water-saturated conditions. Increased hydration can considerably reduce the frictional strength of smectite (Bird, 1984; Morrow et al., 2000). The steady-state coefficient of friction of the powdered natural rocks spans a range from 0.5 to 0.65, at shear velocities over the range 0.1–100 μm/s, and scales negatively with phyllosilicate content (Fig. 4b). The coefficient of friction of the powdered natural rocks does not appear to decrease significantly at water-saturated conditions as in previous studies (Brown et al., 2003; Crawford et al., 2008). A possible explanation is that the phyllosilicates in the natural rocks used in this study are dominantly illite (Table 1); its hydration is typically weaker than that of smectite and this causes an insignificant decrease in the frictional strength of illite-dominated gouges (Ikari et al., 2007; Tembe et al., 2010).

The frictional stability of the two suites of simulated fault gouges was evaluated by the friction parameter $a - b$. Positive values of $a - b$ indicate velocity-strengthening (stable sliding), while negative values imply weakening (potentially unstable slip) (Gu et al., 1984). In Fig. 5, the friction parameter $a - b$ is plotted as a function of phyllosilicate content, for the quartz–smectite mixtures and powdered natural rocks at normal stresses of 20 and 40 MPa. For the quartz–smectite mixtures, an apparent velocity-weakening behavior at phyllosilicate content less than 20 wt.% is observed (Fig. 5a). Initially, $a - b$ for the quartz–smectite mixtures shows an increasing trend with higher phyllosilicate content (normal stress of 20 MPa), but then decreases slightly when the phyllosilicate content is $>$ 50 wt.%. Tembe et al. (2010) also noted a similar trend for binary mixtures of quartz and smectite, and ternary mixtures of quartz, smectite and illite. This trend likely results from localized slip within smectite (Tembe et al., 2010). In comparison, the values of $a - b$ for the quartz–smectite mixtures at higher normal stresses (40 MPa) reach a steady-state at phyllosilicate content $>$30 wt.% (Fig. 5b). For the powdered natural rocks, an increasing trend is observed for $a - b$ values relative to their phyllosilicate contents, at both 20 and 40 MPa. The transition from velocity-weakening to velocity-strengthening for the powdered natural rocks occurs when phyllosilicates are at nearly 15 wt.%, lower than that for the quartz–smectite mixtures.

3.2. Frictional healing

Fault healing is a fundamental process in earthquake physics and is closely related to the recurrence of repeated stick-slip cycles (Karner et al., 1997; Marone, 1997; Olsen et al., 1998). Fault healing rates (β) reflect the rate of fault strength recovery and the requirement for repeated stress drops (Carpenter et al., 2016). Mineralogy also controls frictional healing rates (McLaskey et al., 2012; Tesei et al., 2012). The healing rates of the quartz–smectite mixtures increase slightly, and then decline with increasing phyllosilicate content (Fig. 6a); the lowest healing rates appear for pure smectite gouge, which is consistent with laboratory studies on phyllosilicate bearing gouge (Tesei et al., 2012; Carpenter et al., 2016). For the powdered natural rocks, the healing rates decrease with increasing phyllosilicate content at normal stresses of 10, 20, and 40 MPa. Previous studies have noted that the healing rates for powdered natural rocks also show minor dependence on normal stress (McLaskey et al., 2012).

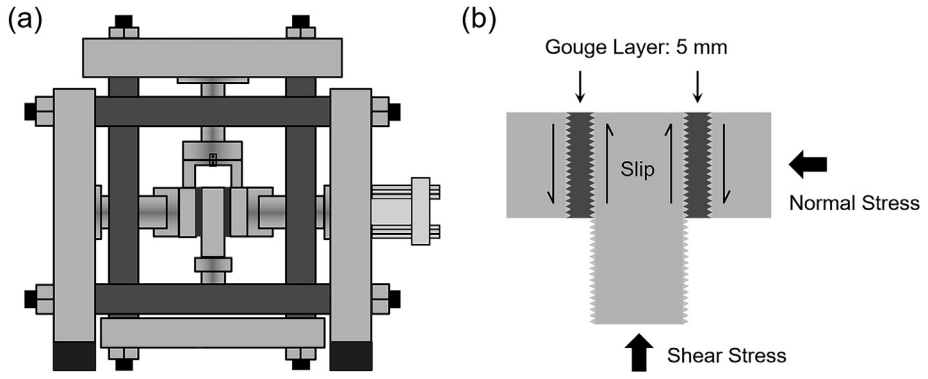

Fig. 1. (a) The biaxial loading frame for friction experiments and (b) the double direct shear configuration with two layers of fault gouge sandwiched between three stainless-steel platens.

3.3. Gouge dilation

The values of gouge dilation are determined using the procedure described in Section 2.2. Fig. 7 shows the variation of gouge dilation with phyllosilicate content for both, the quartz–smectite mixtures and powdered natural rocks, at a normal stress of 20 MPa. Gouge dilation ranges from 0 to 5 μm for the quartz–smectite mixtures, and phyllosilicate-rich gouges tend towards lower values. Comparing the dilation of pure quartz gouge in this study with that of Samuelson et al. (2009) (saturated, but mechanically drained) yields good agreement, despite slight differences in the two experimental testing conditions; our experiments are on dry pure quartz gouge at room humidity. The gouge dilation for the powdered natural rocks exhibits a similar decreasing trend with increasing phyllosilicate content. The values of dilation for the powdered natural rocks are in the range 0–3 μm, noticeably lower than those for the quartz–smectite mixtures. However, these results are consistent with prior work (Kohli and Zoback, 2013) on powdered shale reservoir rocks.

The relationship between gouge dilation and the measured critical slip distance is also examined for the two suites of gouges (Fig. 8). The critical slip distances are positively correlated with gouge dilation and also show strong dependence on phyllosilicate content (Marone and Kilgore, 1993). Meanwhile, dilation decreases slightly with an increase in normal stress (Fig. 9).

3.4. Friction – gouge dilation relationships

The relationships between gouge dilation and frictional strength, stability, and healing are shown in Figs. 10–12, respectively. Dilation increases monotonically with the increase of frictional strength and healing rate. Conversely, an apparent decrease in dilation with increasing frictional stability $a - b$ is observed. When compared with phyllosilicate-poor samples, the phyllosilicate-rich samples tend to exhibit lower frictional strength and healing rate, but higher values of frictional stability $a - b$. Previous studies suggested that gouge dilation is a key factor reflecting fault frictional properties (Kohli and Zoback, 2013; Carpenter et al., 2016). The higher values of gouge dilation reveal that more energy is released with a change in shear velocity for phyllosilicate-poor samples (Carpenter et al., 2016). Therefore, phyllosilicate-poor fault gouges tend to promote unstable slip and higher healing rates.

4. Discussion

The dilation and the relationship of friction–dilation of both suites of gouge are examined and compared with previous studies. The observed friction–dilation is used to infer the permeability evolution in gouge-filled caprock faults.

Table 2
Experimental parameters applied within the suite of experiments on the synthetic gouges. σ_n, applied normal stress; V, shear velocity; t_h, hold time; qtz, quartz; sme, smectite; VS, velocity step; SHS, slide-hold-slide; RH, relative humidity. The friction experiments with the quartz–smectite mixtures and powdered natural rocks were carried out at room humidity and under water-saturated conditions, respectively.

Gouge composition	σ_n (MPa)	Test type	V (μm/s)	t_h (s)	RH
Dataset 1: Mixtures of quartz and smectite powders					
100% qtz	10, 20, 40	VS + SHS	0.3–300	3–300	Room humidity
90% qtz, 10% sme	10, 20, 40	VS + SHS	0.3–300	3–300	Room humidity
80% qtz, 20% sme	10, 20, 40	VS + SHS	0.3–300	3–300	Room humidity
70% qtz, 30% sme	10, 20, 40	VS + SHS	0.3–300	3–300	Room humidity
60% qtz, 40% sme	10, 20, 40	VS + SHS	0.3–300	3–300	Room humidity
50% qtz, 50% sme	10, 20, 40	VS + SHS	0.3–300	3–300	Room humidity
40% qtz, 60% sme	10, 20, 40	VS + SHS	0.3–300	3–300	Room humidity
30% qtz, 70% sme	10, 20, 40	VS + SHS	0.3–300	3–300	Room humidity
20% qtz, 80% sme	10, 20, 40	VS + SHS	0.3–300	3–300	Room humidity
10% qtz, 90% sme	10, 20, 40	VS + SHS	0.3–300	3–300	Room humidity
100% sme	10, 20, 40	VS + SHS	0.3–300	3–300	Room humidity
Dataset 2: Powdered natural rocks					
Daqing volcanic rock	10, 20, 40	VS + SHS	0.1–100	1–1000	Water-saturated
Shengli sandstone	10, 20, 40	VS + SHS	0.1–100	1–1000	Water-saturated
Junggar clasolite	10, 20, 40	VS + SHS	0.1–100	1–1000	Water-saturated
Junggar sandstone	10, 20, 40	VS + SHS	0.1–100	1–1000	Water-saturated
Fuling shale	10, 20, 40	VS + SHS	0.1–100	1–1000	Water-saturated
Changning shale	10, 20, 40	VS + SHS	0.1–100	1–1000	Water-saturated
Chlorite schist	10, 20, 40	VS + SHS	0.1–100	1–1000	Water-saturated

4.1. Comparison with previous studies

Previous experimental studies have extensively explored the role of

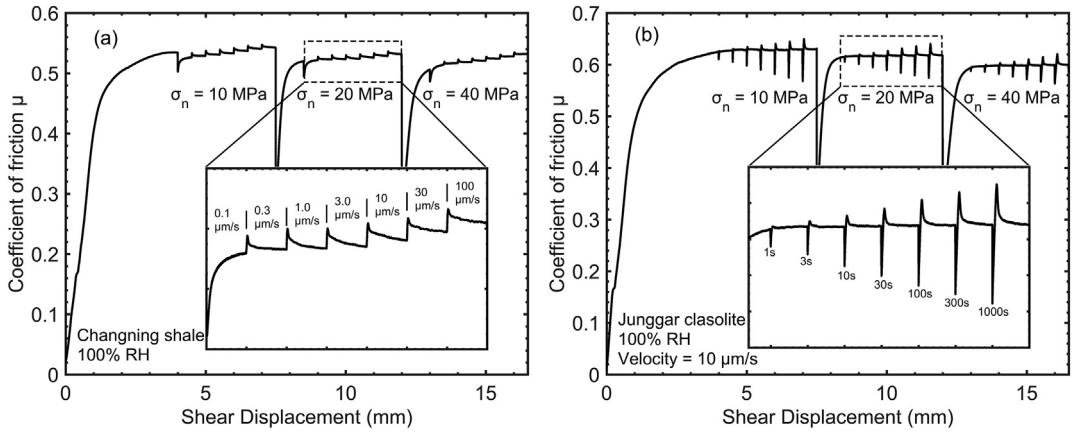

Fig. 2. (a) Representative plots of friction versus shear displacement in velocity-stepping tests at three normal stresses; the inset shows that the shear velocity steps are incremented from 0.1 to 100 μm/s. (b) Typical results for a complete slide-hold-slide test at three normal stresses; the inset shows that the hold time ranges from 1 to 1000 s. RH represents the relative humidity.

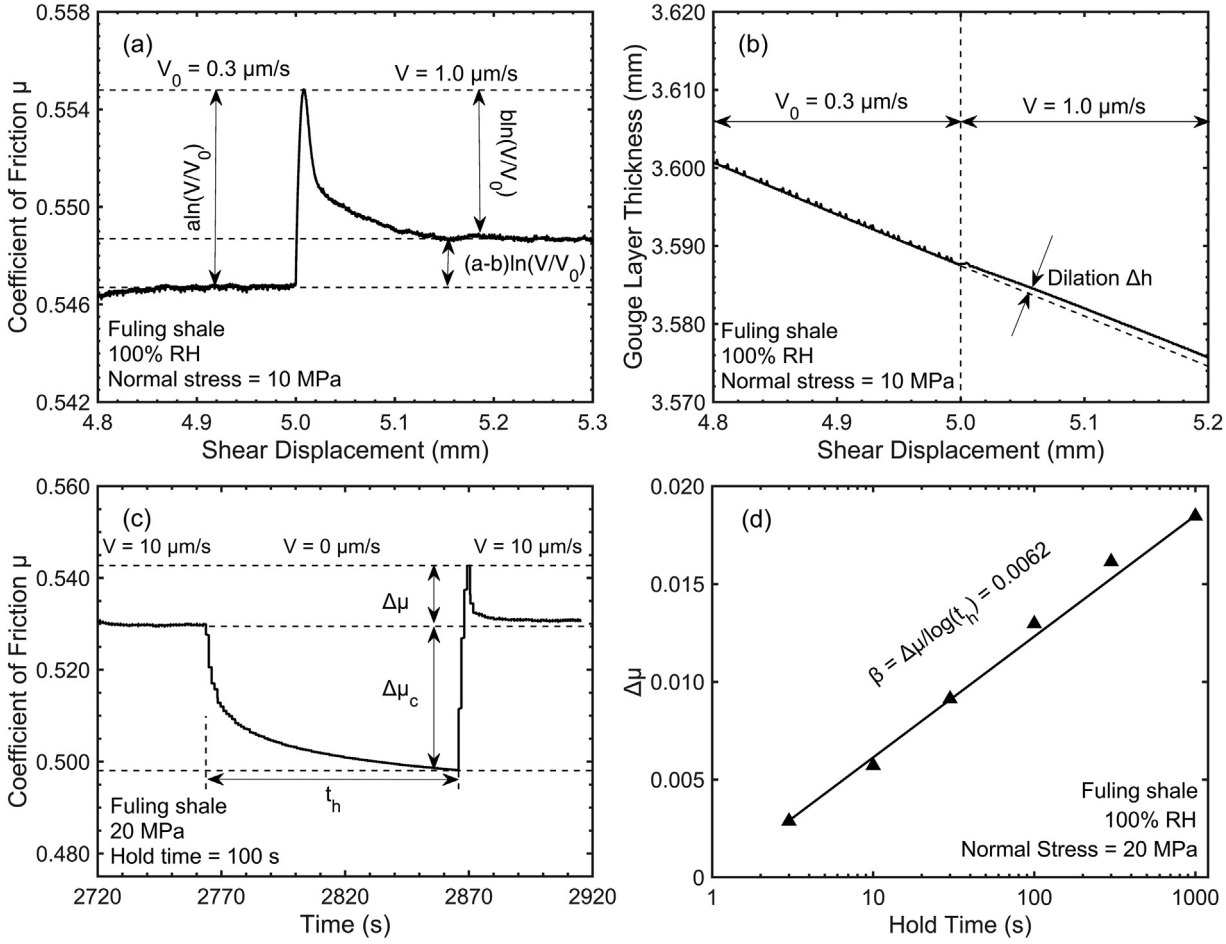

Fig. 3. (a) Definition of frictional stability parameter (a–b) in a velocity-strengthening step; (b) gouge layer thickness change resulting from a velocity step; (c) frictional healing parameters defined in a slide-hold-slide test; and (d) schematic showing the method for calculating frictional healing rate (β). RH represents the relative humidity.

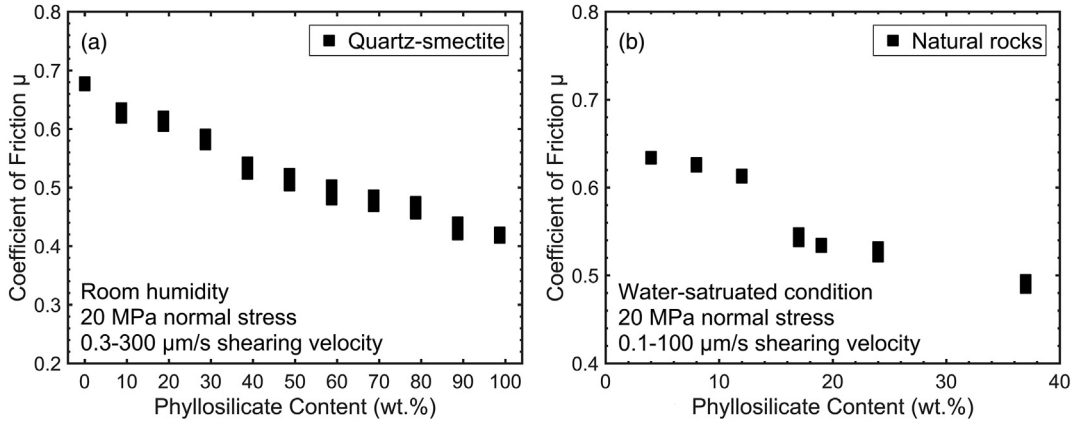

Fig. 4. Steady-state coefficient of friction (μ) as a function of phyllosilicate content in (a) the quartz–smectite mixtures and (b) the natural rocks, at a normal stress of 20 MPa.

mineralogy on frictional properties of tectonic faults, although only a small proportion have systematically examined the role of gouge dilation and its effect on permeability. They suggest that dilation is affected by the state of consolidation and drainage conditions (Morrow and Byerlee, 1989; Marone et al., 1990; Segall and Rice, 1995). Gouge dilation can be positively correlated with critical slip distance (Marone and Kilgore, 1993), and also depends on stress conditions (Ikari et al., 2009; Scuderi et al., 2013); these findings are also supported in this study. The roles of dilatancy and fluid infiltration have also been previously established (Samuelson et al., 2009). Fig. 13 compares gouge dilation versus the coefficient of friction μ and frictional stability $a - b$ from this study with those from Kohli and Zoback (2013); they show good agreement. However, the narrow range of the frictional stability parameter $a - b$ does not allow the results of this study to cover the full spectrum, unlike previous studies. Conversely, dilation of the quartz–smectite mixtures is typically higher than that of the powdered natural rocks. This is most likely a

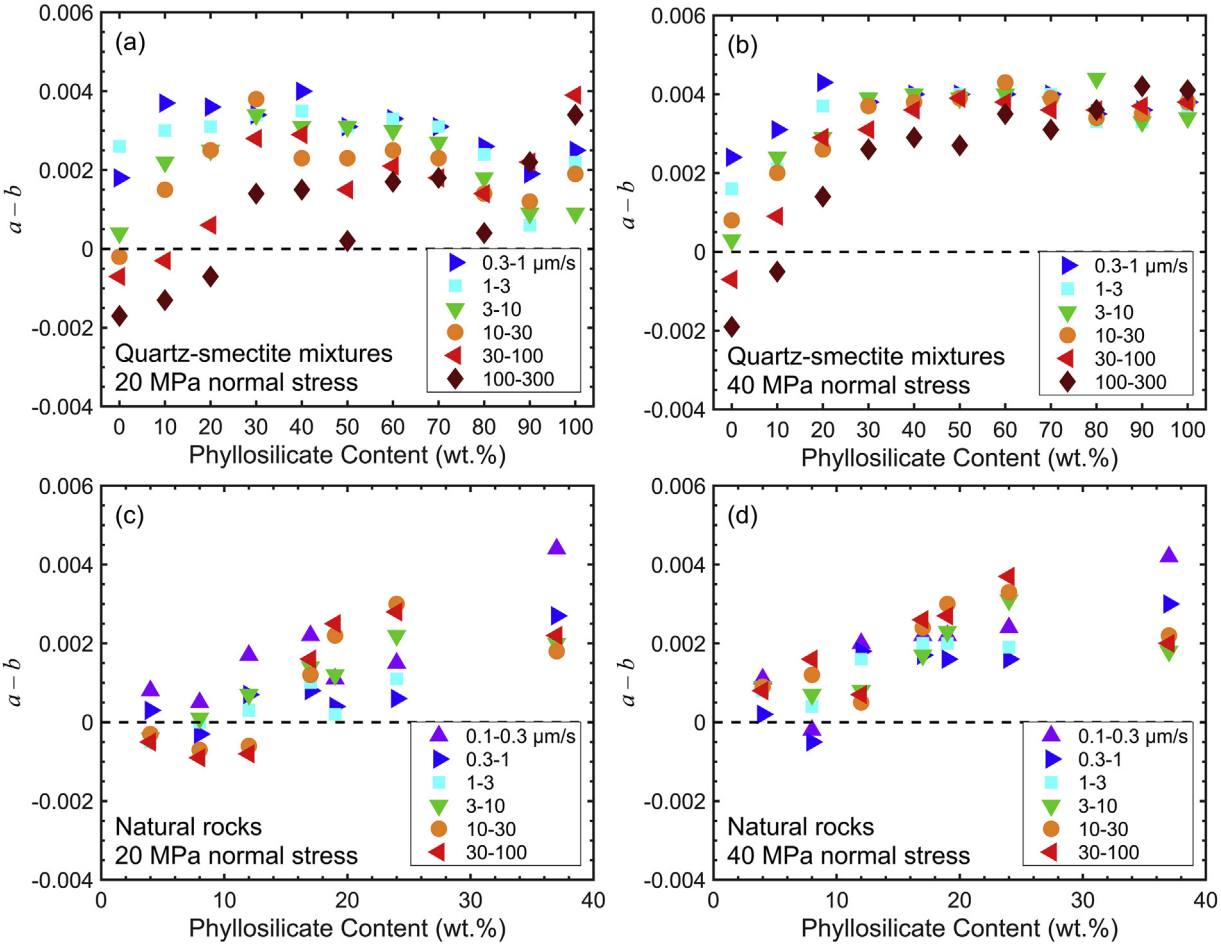

Fig. 5. Velocity dependence of frictional sliding for (a) the quartz–smectite mixtures at a normal stress of 20 MPa; (b) the quartz–smectite mixtures at a normal stress of 40 MPa; (c) the powdered natural rocks at a normal stress of 20 MPa; and (d) the powdered natural rocks at a normal stress of 40 MPa. The legends show the shear velocity in the velocity-stepping tests.

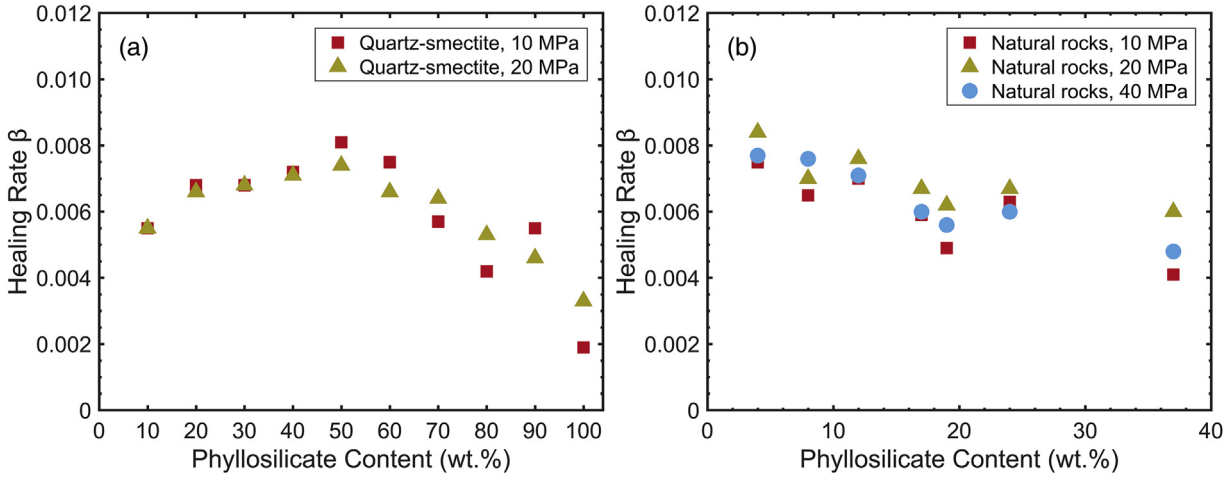

Fig. 6. Frictional healing rates (β) versus phyllosilicate content in (a) the quartz–smectite mixtures under normal stresses of 10 and 20 MPa, and (b) the powdered natural rocks under normal stresses of 10, 20, and 40 MPa.

consequence of conducting the suite of experiments for this study on the quartz–smectite mixtures at room humidity conditions; the corresponding porosity is higher than that of the powdered natural rocks under water-saturated conditions.

4.2. *Implications for permeability evolution of caprock faults*

On the basis of Darcy's law and cubic law for fluid flow, the initial equivalent permeability k_0 for fluid flow through a fault can be calculated as (Ouyang and Elsworth, 1993; Witherspoon et al., 1980; Fang et al., 2018a):

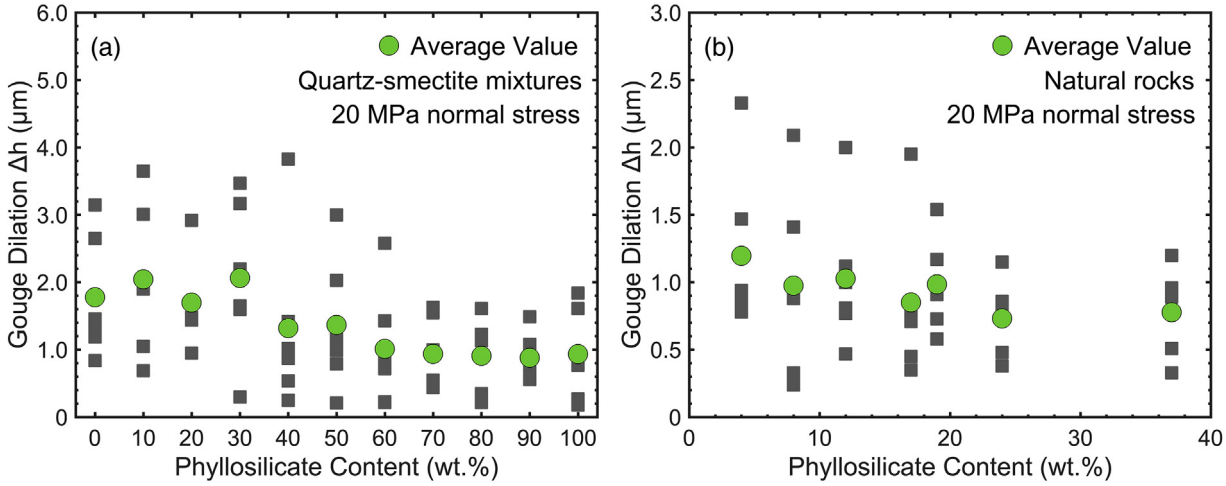

Fig. 7. Gouge dilation (Δh) versus phyllosilicate content for (a) the quartz–smectite mixtures and (b) the powdered natural rocks, at a normal stress of 20 MPa; green circles represent the average dilation values in each test.

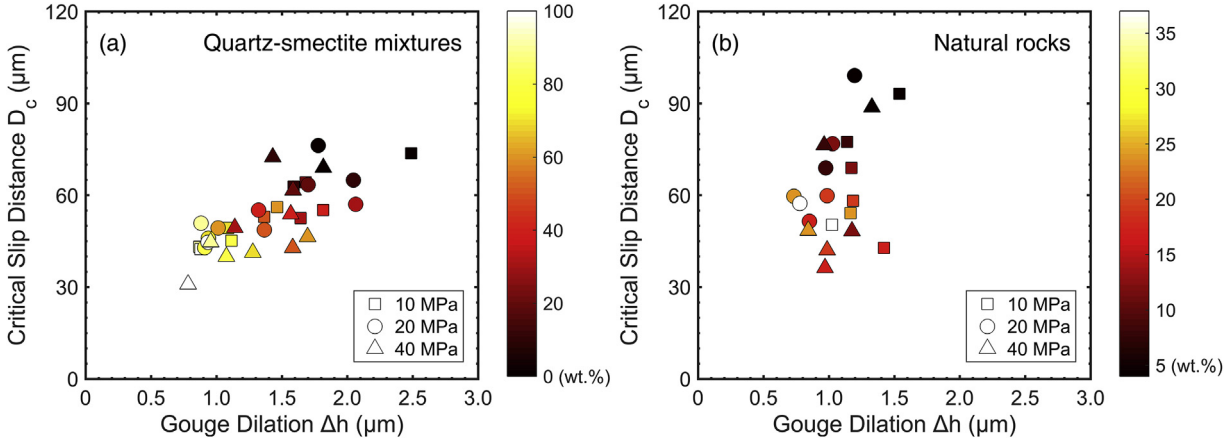

Fig. 8. Measured critical slip distance versus gouge dilation in (a) the quartz–smectite mixtures and (b) the powdered natural rocks at normal stresses of 10, 20, and 40 MPa; the critical slip distance (D_c) and gouge dilation (Δh) represent the average value in a single test. Colored bars show the phyllosilicate content for each sample.

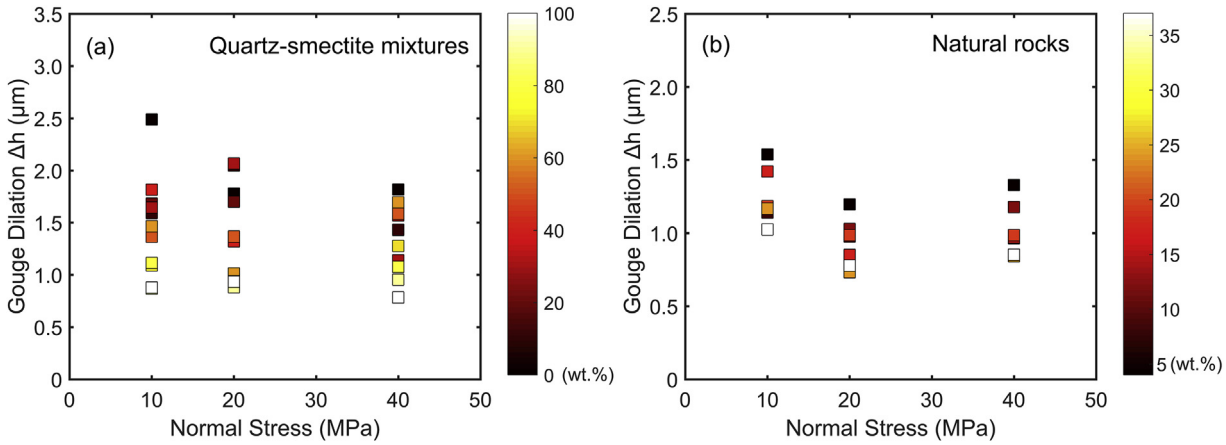

Fig. 9. Measured gouge dilation as a function of normal stress for (a) the quartz–smectite mixtures and (b) the powdered natural rocks; only average values of gouge dilation in each test are plotted. The colored bars on the right indicate phyllosilicate content.

$$k_0 = \frac{\mu L Q}{b_0 W \Delta P_f} = \frac{b_0^2}{12} \quad (6)$$

where μ is the fluid viscosity, L represents the length of the flow path, Q is the flow rate, b_0 is the initial fault aperture, W denotes the initial fault width, and ΔP_f is the pressure difference across the fault. If the fault aperture is increased by Δb, the new permeability k can be related to k_0 by (Samuelson et al., 2011; Im et al., 2018):

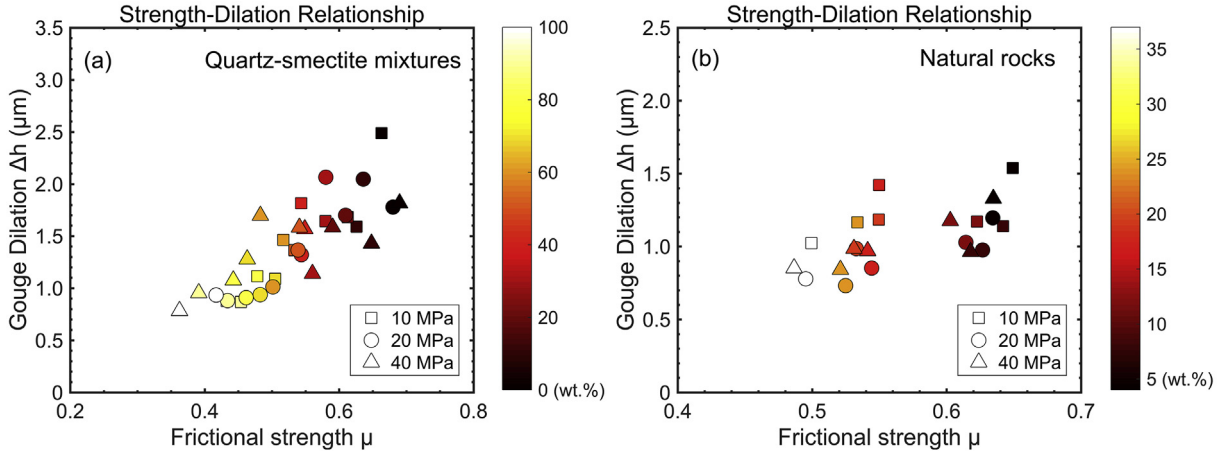

Fig. 10. Frictional strength–gouge dilation relationship for (a) the quartz–smectite mixtures and (b) the powdered natural rocks at normal stresses of 10, 20, and 40 MPa. Frictional strength (μ) is determined at a shear velocity of 10 μm/s for the quartz–smectite mixtures, and a shear velocity of 3 μm/s for the powdered natural rocks. The colored bars indicate phyllosilicate content.

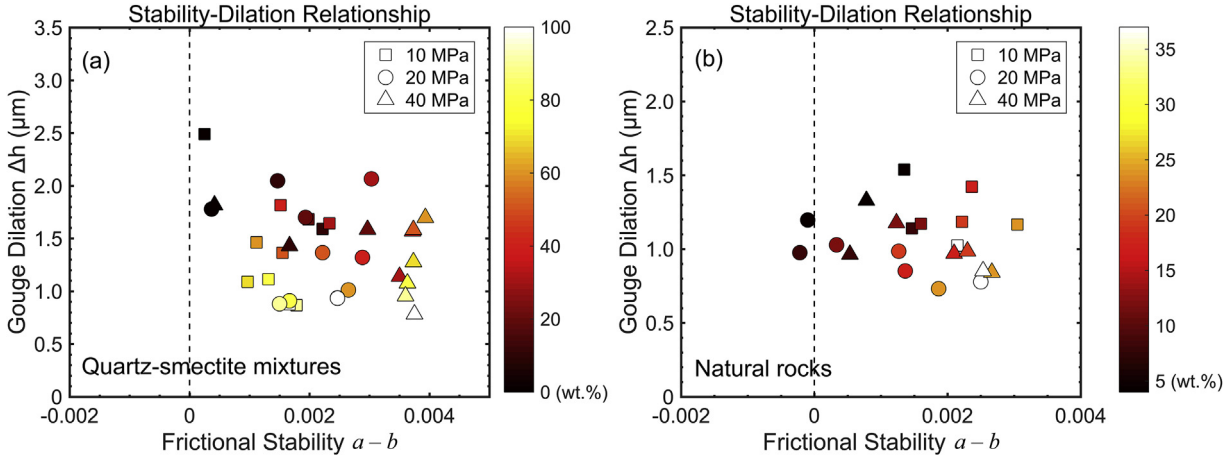

Fig. 11. Frictional stability–gouge dilation relationship for (a) the quartz–smectite mixtures and (b) the powdered natural rocks at normal stresses of 10, 20, and 40 MPa; an average value of the frictional stability parameter (a–b) is adopted in each shear experiment for comparison. Colored bars indicate phyllosilicate content.

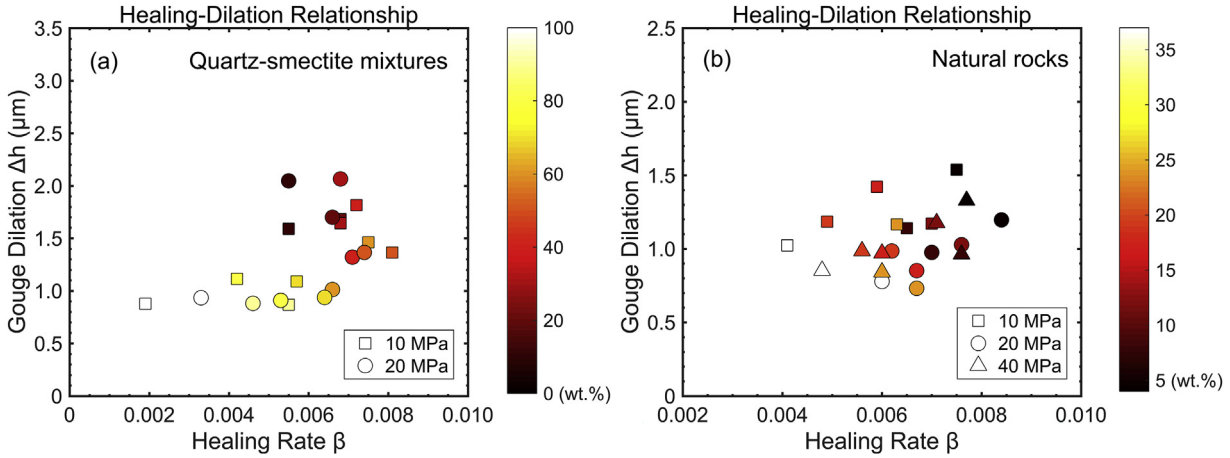

Fig. 12. Frictional healing–gouge dilation relationship for (a) the quartz–smectite mixtures and (b) the powdered natural rocks at normal stresses of 10, 20, and 40 MPa. Colored bars indicate phyllosilicate content.

$$\frac{k}{k_0}=\left(\frac{b_0+\Delta b}{b_0}\right)^2=\left(1+\frac{\Delta b}{b_0}\right)^2 \quad (7)$$

In this study, the fault aperture incrementation Δb relative to the initial fault aperture b_0 is equivalent to the gouge dilation Δh relative to the initial gouge thickness h (Samuelson et al., 2009). Consequently, Eq. (7) can be rewritten as:

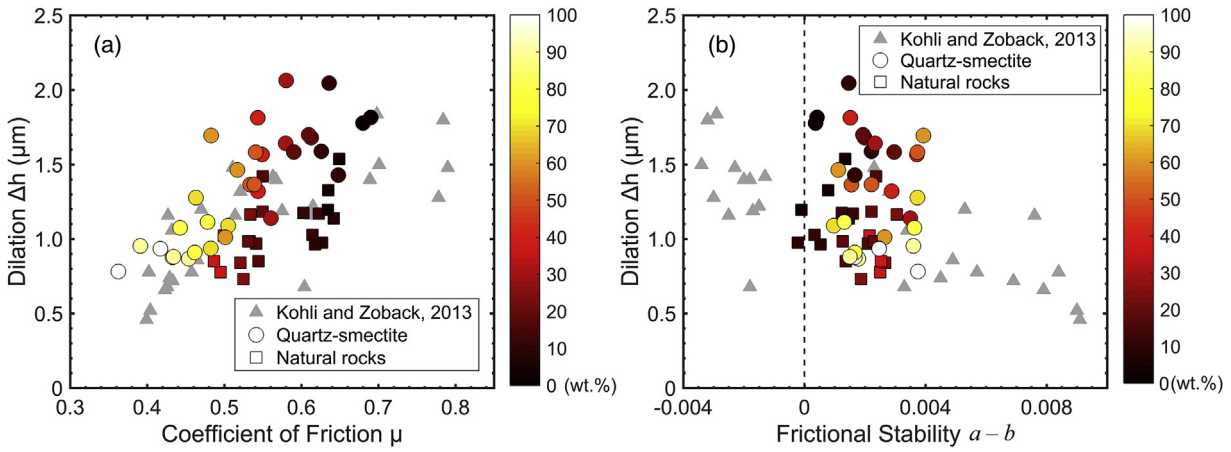

Fig. 13. Relationships of gouge dilation with (a) coefficient of friction μ and (b) frictional stability (a–b) for both, the quartz–smectite mixtures and powdered natural rocks; only average values are shown here. The grey triangles represent results from Kohli and Zoback (2013). Colored bars indicate phyllosilicate content.

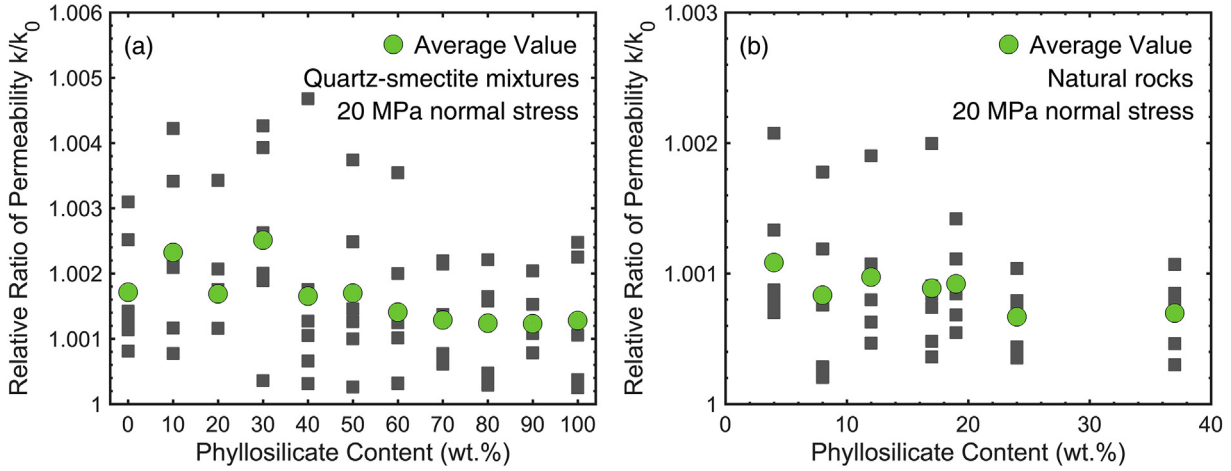

Fig. 14. Normalized apparent permeability (k/k_0) versus phyllosilicate content for (a) the quartz–smectite mixtures and (b) the powdered natural rocks at a normal stress of 20 MPa; green circles indicate the average change in permeability values in a single experiment.

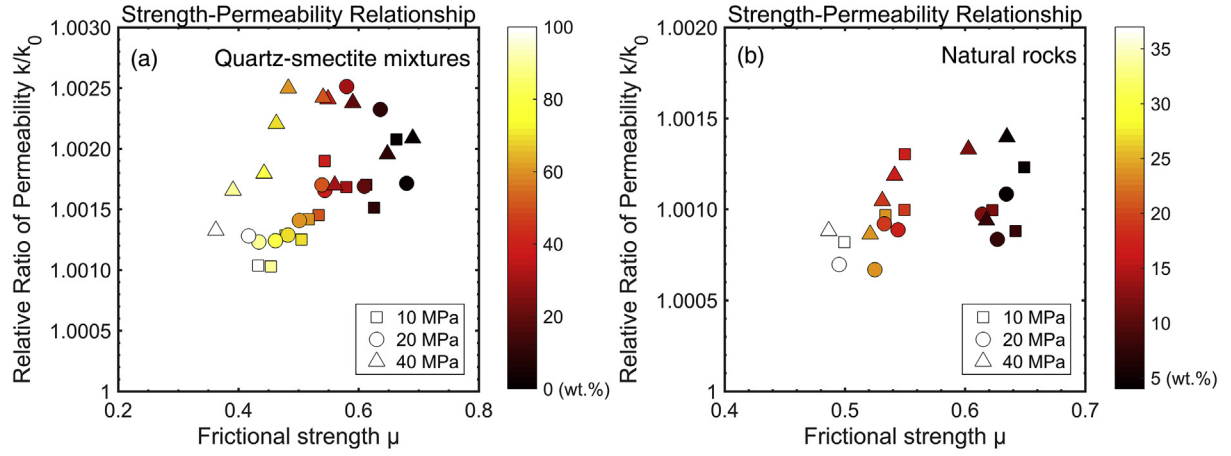

Fig. 15. Frictional strength–permeability relationship for (a) the quartz–smectite mixtures and (b) the powdered natural rocks at normal stresses of 10, 20, and 40 MPa. Frictional strength (μ) is evaluated at a shear velocity of 10 μm/s for the quartz–smectite mixtures, and at 3 μm/s for the powdered natural rocks. Colored bars indicate phyllosilicate content.

$$\frac{k}{k_0} = \left(1 + \frac{\Delta b}{b_0}\right)^2 = \left(1 + \frac{\Delta h}{h}\right)^2 \quad (8)$$

Equation (8) is used to infer the change in apparent permeability, and Fig. 14 shows the apparent change in permeability versus the phyllosilicate content for the two suites of gouges at a normal stress of 20 MPa. Unsurprisingly, in the case where permeability change neglects any nonlinear effects of grain comminution or particulate mobilization, the

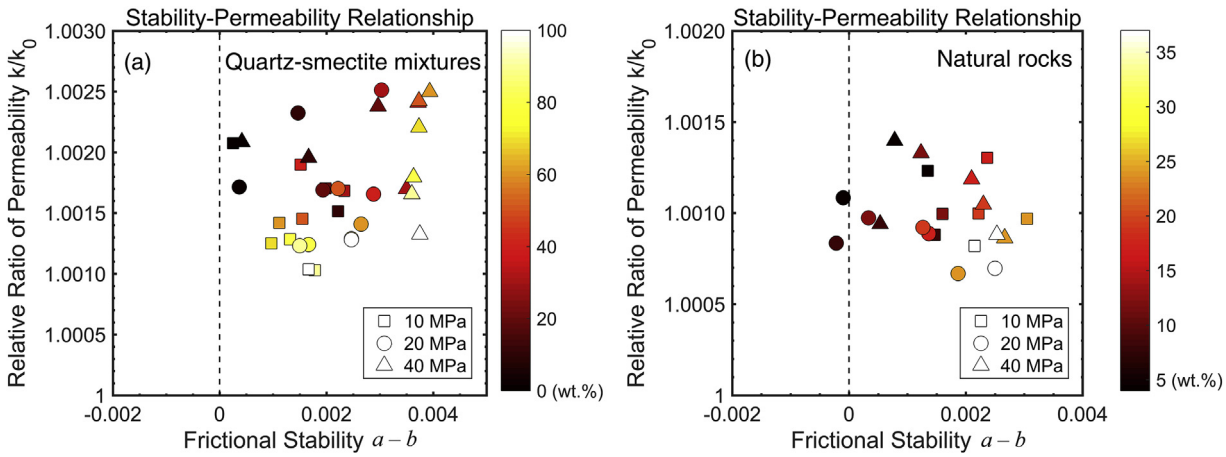

Fig. 16. Frictional stability–permeability relationship for (a) the quartz–smectite mixtures and (b) the powdered natural rocks at normal stresses of 10, 20, and 40 MPa. The frictional stability parameter (a–b) represents the average value in each shear experiment. Colored bars denote phyllosilicate content.

permeability evolution versus phyllosilicate content relationship is similar to the relationship of gouge dilation – phyllosilicate content.

The relative permeability values for phyllosilicate-rich gouges in this study are congruent to previous experiments which measured permeability directly (Yasuhara et al., 2004; Ishibashi et al., 2013; Fang et al., 2017a, 2018b; Wang et al., 2017). However, the results for permeability evolution for phyllosilicate-poor gouges in this study are typically lower than previous observations. A possible reason for this discrepancy is due to the difference of gouge grain-sizes, and the impact of grain comminution and clogging. Samuelson et al. (2009) suggested that the change in gouge porosity ($\Delta\phi$) is equivalent to the gouge dilation relative to the initial gouge thickness measured in double direct shear experiments. The quartz–smectite mixtures and powdered natural rocks in this study span a broad grain-size distribution. For instance, grain-size analysis indicates that the powdered Fuling shale ranges from 0.131 to 164.331 μm. The voids between coarse grains are filled by finer grains; thus, the porosity may change slightly during shearing compared with previous studies (Ishibashi et al., 2013; Fang et al., 2017a).

Since the frictional strength, stability, healing, and permeability of both, the quartz–smectite mixtures and powdered natural rocks, scale with phyllosilicate content, the relationships between permeability and fault strength, stability, and healing may also be established (Figs. 15–17). The permeability ratio k/k_0 is positively correlated with frictional strength μ and healing rate β, but negatively correlated with frictional stability $a - b$. This is consistent with previous laboratory measurements and numerical simulations on stability–permeability relationships by Fang et al. (2017a), Wang et al. (2017), and Wu et al. (2017). Phyllosilicate-poor gouge samples typically have higher frictional strength and healing rate, and promote potentially unstable slip, but show a higher permeability upon the velocity change during shearing.

The mechanical integrity, low permeability, and high entry pressures of caprocks are necessary for the integrity of water and CO_2 injection reservoirs (Vilarrasa et al., 2011; Hou et al., 2012; Corrado et al., 2014). However, the presence of pre-existing faults and fractures can significantly change the permeability of caprocks. This study shows that for faults filled with phyllosilicate-poor gouge, unstable and dynamic slip is readily arrested during fault reactivation. The friction–permeability relationships further indicate that the reactivation of faults filled with phyllosilicate-poor gouge undergo significant dilation, leading to an increase in permeability. Meanwhile, high healing rates reflect rapid stress recovery upon dynamic slip, rapidly decreasing gouge dilation. The inference here is that although the reactivation of faults with phyllosilicate-poor gouge can increase permeability, high healing rates may accelerate a decreasing rate of permeability during rapid dynamic slip. Thus, the reactivation of caprock faults with phyllosilicate-poor gouge may have a negligible influence on permeability evolution.

5. Conclusions

This study systematically investigates the role of mineralogy on gouge dilation and frictional strength, stability, and healing relationships for a

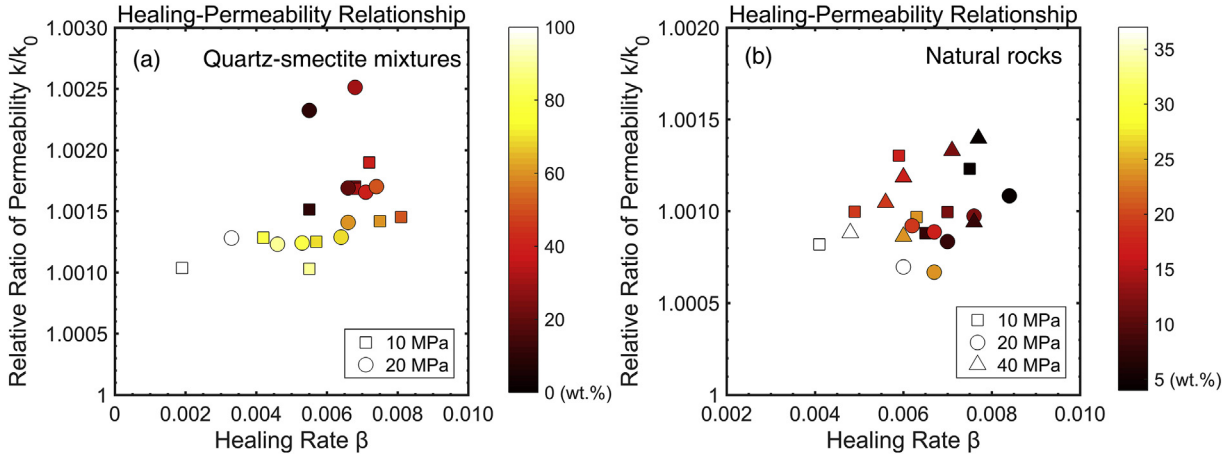

Fig. 17. Frictional healing–permeability relationship for (a) the quartz–smectite mixtures; and (b) the powdered natural rocks at normal stresses of 10, 20, and 40 MPa. Colored bars show phyllosilicate content.

suite of synthetic gouges, quartz–smectite mixtures and powdered natural rocks. Velocity-stepping and slide-hold-slide experiments were conducted to measure frictional stability and healing rates, respectively. The friction–dilation relationship is applied to define the permeability evolution of caprock faults and evaluate the change of normalized apparent permeability. The conclusions drawn from this study are:

(1) The frictional strength of both suites of gouges systematically decrease with increasing phyllosilicate content.
(2) Frictional stability measurements indicate a transition from velocity-weakening (potentially unstable slips) to velocity-strengthening (stable sliding) at about 20 wt.% phyllosilicate content for both gouges. The frictional stability parameter $a - b$ monotonically increases for the powdered natural rocks, but plateaus at higher phyllosilicate contents for the quartz–smectite mixtures. When compared with phyllosilicate-rich samples, the phyllosilicate-poor gouges generally show higher healing rates.
(3) Gouge dilation shows an overall decreasing trend with increasing phyllosilicate content for both suites of gouges. Fault gouge dilation also shows a strong dependence on critical slip distance and stress conditions. The friction–dilation relationships suggest that gouge dilation is positively correlated with frictional strength and healing rates, and negatively correlated to frictional stability.
(4) Fault reactivation may have a negligible influence on permeability change for phyllosilicate-poor gouge-bearing caprock faults.

Acknowledgements

The research is supported by the National Natural Science Foundation of China (Nos. 41672268 and 41772286), the PetroChina Innovation Foundation (2018D-5007-0202) and the US Department of Energy (DE-FE0023354). Discussions with Chris Marone and Changrong He are greatly appreciated.

References

Bird, P., 1984. Hydration-phase diagrams and friction of montmorillonite under laboratory and geologic conditions, with implications for shale compaction, slope stability, and strength of fault gouge. Tectonophysics 107 (3), 235–260.
Boulton, C., Yao, L., Faulkner, D.R., Townend, J., Toy, V.G., Sutherland, R., et al., 2017. High-velocity frictional properties of Alpine Fault rocks: mechanical data, microstructural analysis, and implications for rupture propagation. J. Struct. Geol. 97, 71–92.
Brown, K.M., Kopf, A., Underwood, M.B., Weinberger, J.L., 2003. Compositional and fluid pressure controls on the state of stress on the Nankai subduction thrust: a weak plate boundary. Earth Planet. Sci. Lett. 214 (3), 589–603.
Carpenter, B.M., Ikari, M.J., Marone, C., 2016. Laboratory observations of time-dependent frictional strengthening and stress relaxation in natural and synthetic fault gouges. J. Geophys. Res. Solid Earth 121 (2), 1183–1201.
Chen, J., Verberne, B.A., Spiers, C.J., 2015. Effects of healing on the seismogenic potential of carbonate fault rocks: experiments on samples from the Longmenshan Fault, Sichuan, China. J. Geophys. Res. Solid Earth 120 (8), 5479–5506.
Collettini, C., Niemeijer, A., Viti, C., Marone, C., 2009. Fault zone fabric and fault weakness. Nature 462 (7275), 907–910.
Corrado, S., Aldega, L., Celano, A.S., Benedetti, A. A. De, Giordano, G., 2014. Cap rock efficiency and fluid circulation of natural hydrothermal systems by means of XRD on clay minerals (Sutri, Northern Latium, Italy). Geothermics 50 (115), 180–188.
Crawford, B.R., Faulkner, D.R., Rutter, E.H., 2008. Strength, porosity, and permeability development during hydrostatic and shear loading of synthetic quartz-clay fault gouge. J. Geophys. Res. Solid Earth 113, B03207. https://doi.org/10.1029/2006JB004634.
Dieterich, J.H., 1978. Time-dependent friction and the mechanics of stick-slip. Pure Appl. Geophys. 116 (4–5), 790–806.
Dieterich, J.H., 1979. Modeling of rock friction: 1. Experimental results and constitutive equations. J. Geophys. Res. 84 (B5), 2161–2168.
Elsworth, D., Spiers, C.J., Niemeijer, A.R., 2016. Understanding induced seismicity. Science 354 (6318), 1380–1381.
Fang, Y., Elsworth, D., Wang, C., Ishibashi, T., Fitts, J.P., 2017a. Frictional stability-permeability relationships for fractures in shales. J. Geophys. Res. Solid Earth 122 (3), 1760–1776.
Fang, Y., Wang, C., Elsworth, D., Ishibashi, T., 2017. Seismicity-permeability coupling in the behavior of gas shales, CO_2 storage and deep geothermal energy. Geomech. Geophys. Geo-Energy Geo-Resources 3 (2), 1–10.
Fang, Y., Elsworth, D., Cladouhos, T.T., 2018. Reservoir permeability mapping using microearthquake data. Geothermics 72, 83–100.
Fang, Y., Elsworth, D., Wang, C., Jia, Y., 2018. Mineralogical controls on frictional strength, stability, and shear permeability evolution of fractures. J. Geophys. Res. Solid Earth 123, 3549–3563.
Faoro, I., Niemeijer, A., Marone, C., Elsworth, D., 2009. Influence of shear and deviatoric stress on the evolution of permeability in fractured rock. J. Geophys. Res. Solid Earth 114 (1), 1–10.
Faulkner, D.R., Jackson, C.A.L., Lunn, R.J., Schlische, R.W., Shipton, Z.K., Wibberley, C.A.J., Withjack, M.O., 2010. A review of recent developments concerning the structure, mechanics and fluid flow properties of fault zones. J. Struct. Geol. 32 (11), 1557–1575.
Frye, K.M., Marone, C., 2002. Effect of humidity on granular friction at room temperature. J. Geophys. Res. Solid Earth 107 (B11), 2309. https://doi.org/10.1029/2001JB000654.
Grigoli, F., Cesca, S., Rinaldi, A.P., Manconi, A., López-Comino, J.A., Clinton, J.F., Westaway, R., Cauzzi, C., Dahm, T., Wiemer, S., 2018. The November 2017 M_w 5.5 Pohang earthquake: a possible case of induced seismicity in South Korea. Science 360 (6392), 1003–1006.
Gu, J.C., Rice, J.R., Ruina, A.L., Tse, S.T., 1984. Slip motion and stability of a single degree of freedom elastic system with rate and state friction. J. Mech. Phys. Solids 32 (3), 167–196.
Guglielmi, Y., Elsworth, D., Cappa, F., Henry, P., Gout, C., Dick, P., Durand, J., 2015. In situ observations on the coupling between hydraulic diffusivity and displacements during fault reactivation in shales. J. Geophys. Res. Solid Earth 120 (11), 7729–7748.
Han, R., Shimamoto, T., Ando, J., Ree, J., 2007. Seismic slip record in carbonate-bearing fault zones: an insight from high-velocity friction experiments on siderite gouge. Geology 35 (12), 1131–1134.
Hou, Z., Rockhold, M.L., Murray, C.J., 2012. Evaluating the impact of caprock and reservoir properties on potential risk of CO_2 leakage after injection. Environ. Earth Sci. 66 (8), 2403–2415.
Hunfeld, L.B., Niemeijer, A.R., Spiers, C.J., 2017. Frictional properties of simulated fault gouges from the seismogenic Groningen Gas Field under in situ P–T -chemical conditions. J. Geophys. Res. Solid Earth 122 (11), 8969–8989.
Ikari, M.J., Saffer, D.M., Marone, C., 2007. Effect of hydration state on the frictional properties of montmorillonite-based fault gouge. J. Geophys. Res. Solid Earth 112 (6), 1–12.
Ikari, M.J., Saffer, D.M., Marone, C., 2009. Frictional and hydrologic properties of clay-rich fault gouge. J. Geophys. Res. 114, B05409. https://doi.org/10.1029/2008JB006089.
Ikari, M.J., Marone, C., Saffer, D.M., 2011. On the relation between fault strength and frictional stability. Geology 39 (1), 83–86.
Im, K., Elsworth, D., Fang, Y., 2018. The influence of preslip sealing on the permeability evolution of fractures and faults. Geophys. Res. Lett. 45 (1), 166–175.
Ishibashi, T., Mcguire, T.P., Watanabe, N., Tsuchiya, N., Elsworth, D., 2013. Permeability evolution in carbonate fractures: competing roles of confining stress and fluid pH. Water Resour. Res. 49 (5), 2828–2842.
Johnson, P.A., Savage, H., Knuth, M., Gomberg, J., Marone, C., 2008. Effects of acoustic waves on stick-slip in granular media and implications for earthquakes. Nature 451 (7174), 57–60.
Karner, S.L., Marone, C., Evans, B., 1997. Laboratory study of fault healing and lithification in simulated fault gouge under hydrothermal conditions. Tectonophysics 277 (1–3), 41–55.
Kawamoto, E., Shimamoto, T., 1998. The strength profile for bimineralic shear zones: an insight from high-temperature shearing experiments on calcite–halite mixtures. Tectonophysics 295 (295), 1–14.
Kohli, A.H., Zoback, M.D., 2013. Frictional properties of shale reservoir rocks. J. Geophys. Res. Solid Earth 118 (9), 5109–5125.
Kim, K.H., Ree, J.H., Kim, Y.H., Kim, S., Kang, S.Y., Seo, W., 2018. Assessing whether the 2017 M_w 5.4 Pohang earthquake in South Korea was an induced event. Science 1–6.
Logan, J.M., Rauenzahn, K.A., 1987. Frictional dependence of gouge mixtures of quartz and montmorillonite on velocity, composition and fabric. Tectonophysics 144 (1–3), 87–108.
Marone, C., 1997. On the rate of frictional healing and the constitutive law for time- and slip-dependent friction. Int. J. Rock Mech. Min. Sci. Geomech. Abstr. 34 (3–4), 347.
Marone, C., 1998. Laboratory-derived friction laws and their application to seismic faulting. Annu. Rev. Earth Planet Sci. 26 (1), 643–696.
Marone, C., Kilgore, B., 1993. Scaling of the critical slip distance for seismic faulting with shear strain in fault zones. Nature 362 (6421), 618–621.
Marone, C., Raleigh, C.B., Scholz, C.H., 1990. Frictional behavior and constitutive modeling of simulated fault gouge. J. Geophys. Res. Solid Earth 95 (B5), 7007–7025.
McLaskey, G.C., Thomas, A.M., Glaser, S.D., Nadeau, R.M., 2012. Fault healing promotes high-frequency earthquakes in laboratory experiments and on natural faults. Nature 491 (7422), 101–104.
Moore, D.E., Lockner, D.A., 2011. Frictional strengths of talc-serpentine and talc-quartz mixtures. J. Geophys. Res. Solid Earth 116, B01403. https://doi.org/10.1029/2010JB007881.
Morrow, C.A., Byerlee, J.D., 1989. Experimental studies of compaction and dilatancy during frictional sliding on faults containing gouge. J. Struct. Geol. 11 (7), 815–825.
Morrow, C.A., Moore, D.E., Lockner, D.A., 2000. The effect of mineral bond strength and adsorbed water on fault gouge frictional strength. Geophys. Res. Lett. 27 (6), 815–818.
Niemeijer, A.R., Spiers, C.J., 2006. Velocity dependence of strength and healing behaviour in simulated phyllosilicate-bearing fault gouge. Tectonophysics 427 (1), 231–253.
Olsen, M.P., Scholz, C.H., Léger, A., 1998. Healing and sealing of a simulated fault gouge under hydrothermal conditions: implications for fault healing. J. Geophys. Res. 103 (B4), 7421.

Ouyang, Z., Elsworth, D., 1993. Evaluation of groundwater flow into mined panels. Int. J. Rock Mech. Min. Sci. 30 (2), 71–79.
Ruina, A., 1983. Slip instability and state variable friction laws. J. Geophys. Res. Solid Earth 88 (B12), 10359–10370.
Rutqvist, J., Birkholzer, J., Cappa, F., Tsang, C.F., 2007. Estimating maximum sustainable injection pressure during geological sequestration of CO_2 using coupled fluid flow and geomechanical fault-slip analysis. Energy Convers. Manag. 48 (6), 1798–1807.
Saffer, D.M., Marone, C., 2003. Comparison of smectite- and illite-rich gouge frictional properties: application to the updip limit of the seismogenic zone along subduction megathrusts. Earth Planet. Sci. Lett. 215 (1–2), 219–235.
Samuelson, J., Marone, C., Voight, B., Elsworth, D., 2008. Laboratory investigation of the frictional behavior of granular volcanic material. J. Volcanol. Geotherm. Res. 173 (3–4), 265–279.
Samuelson, J., Elsworth, D., Marone, C., 2009. Shear-induced dilatancy of fluid-saturated faults: experiment and theory. J. Geophys. Res.: Solid Earth 114 (12), 1–15.
Samuelson, J., Elsworth, D., Marone, C., 2011. Influence of dilatancy on the frictional constitutive behavior of a saturated fault zone under a variety of drainage conditions. J. Geophys. Res. Solid Earth 116 (10), 1–17.
Scuderi, M.M., Niemeijer, A.R., Collettini, C., Marone, C., 2013. Frictional properties and slip stability of active faults within carbonate-evaporite sequences: the role of dolomite and anhydrite. Earth Planet. Sci. Lett. 369–370, 220–232.
Scuderi, M.M., Carpenter, B.M., Marone, C., 2014. Physicochemical processes of frictional healing: effects of water on stick-slip stress drop and friction of granular fault gouge. J. Geophys. Res. Solid Earth 119 (5), 4090–4105.
Segall, P., Rice, J.R., 1995. Dilatancy, compaction, and slip instability of a fluid-infiltrated fault. J. Geophys. Res. Solid Earth 100 (B11), 22155–22171.
Shapiro, S.A., Dinske, C., Rothert, E., 2006. Hydraulic-fracturing controlled dynamics of microseismic clouds. Geophys. Res. Lett. 33, L14312. https://doi.org/10.1029/2006GL026365.
Suckale, J., 2009. Induced seismicity in hydrocarbon fields. Adv. Geophys. 51 (C), 55–106.
Takahashi, M., Mizoguchi, K., Kitamura, K., Masuda, K., 2007. Effects of clay content on the frictional strength and fluid transport property of faults. J. Geophys. Res. 112, B08206. https://doi.org/10.1029/2006JB004678.
Tembe, S., Lockner, D.A., Wong, T.-F., 2010. Effect of clay content and mineralogy on frictional sliding behavior of simulated gouges: binary and ternary mixtures of quartz, illite, and montmorillonite. J. Geophys. Res. 115, B03416. https://doi.org/10.1029/2009JB006383.
Tesei, T., Collettini, C., Carpenter, B.M., Viti, C., Marone, C., 2012. Frictional strength and healing behavior of phyllosilicate-rich faults. J. Geophys. Res. 117 (9), 1–13.
Vilarrasa, V., Olivella, S., Carrera, J., 2011. Geomechanical stability of the caprock during CO_2 sequestration in deep saline aquifers. Energy Procedia 4 (22), 5306–5313.
Wang, C., Elsworth, D., Fang, Y., 2017. Influence of weakening minerals on ensemble strength and slip stability of faults. J. Geophys. Res. Solid Earth 122 (9), 7090–7110. https://doi.org/10.1002/2016JB013687.
Witherspoon, P.A., Wang, J.S.Y., Iwai, K., Gale, J.E., 1980. Validity of cubic law for fluid flow in a deformable rock fracture. Water Resour. Res. 16 (6), 1016–1024.
Wu, W., Reece, J.S., Gensterblum, Y., Zoback, M.D., 2017. Permeability evolution of slowly slipping faults in shale reservoirs. Geophys. Res. Lett. 44 (24), 11,368–11,375. https://doi.org/10.1002/2017GL075506.
Yang, D.S., Wang, W., Chen, W.Z., Tan, X.J., Wang, L.G., 2019. Revisiting the methods for gas permeability measurement in tight porous medium. J. Rock mech. Geotech. Eng. 11 (2), 263–276.
Yasuhara, H., Elsworth, D., Polak, A., 2004. Evolution of permeability in a natural fracture: significant role of pressure solution. J. Geophys. Res. Solid Earth 109, B03204. https://doi.org/10.1029/2003JB002663.
Ye, Z., Janis, M., Ghassemi, A., Riley, S., 2017. Laboratory investigation of fluid flow and permeability evolution through pre-existing shale fractures. In: Unconventional Resources Technology Conference, Austin, Texas, 24–26 July 2017. Society of Exploration Geophysicists, American Association of Petroleum Geologists, Society of Petroleum Engineers, 2038–2052.
Zhang, F., An, M., Zhang, L., Fang, Y., Elsworth, D., 2019. The role of mineral composition on the frictional and stability properties of powdered reservoir rocks. J. Geophys. Res. Solid Earth 124 (2), 1480–1497.
Zhong, Z., Elsworth, D., Hu, Y., 2016. Evolution of strength and permeability in stressed fractures with fluid–rock interactions. Pure Appl. Geophys. 173 (2), 525–536.